THE JOURNAL OF BIOLOGICAL CHEMISTRY VOL. 287, NO. 40, pp. 33905–33916, September 28, 2012
© 2012 by The American Society for Biochemistry and Molecular Biology, Inc. Published in the U.S.A.

On the Roles and Regulation of Chondroitin Sulfate and Heparan Sulfate in Zebrafish Pharyngeal Cartilage Morphogenesis*[S]

Received for publication, July 16, 2012 Published, JBC Papers in Press, August 6, 2012, DOI 10.1074/jbc.M112.401646

Katarina Holmborn[‡1], Judith Habicher[§1], Zsolt Kasza[‡], Anna S. Eriksson[‡], Beata Filipek-Gorniok[‡], Sandeep Gopal[¶2], John R. Couchman[¶2], Per E. Ahlberg[‡], Malgorzata Wiweger[‖3], Dorothe Spillmann[‡], Johan Kreuger[‡4,5], and Johan Ledin[§4,6]

From the [‡]Department of Medical Biochemistry and Microbiology, Science for Life Laboratory, Uppsala University, Husargatan 3, SE-751 23, Uppsala, Sweden, the [§]Department of Organism Biology, Science for Life Laboratory, Uppsala University, Norbyvägen 18A, SE-752 36 Uppsala, Sweden, the [¶]Department of Biomedical Sciences, University of Copenhagen, 2200 Copenhagen N, Denmark, and the [‖]Department of Pathology, Leiden University Medical Centre, 2300 RC Leiden, The Netherlands

Background: Chondroitin sulfate (CS) and heparan sulfate (HS) are important for cartilage formation.
Results: Analyses of zebrafish mutants demonstrate interplay between HS and CS biosynthesis *in vivo*.
Conclusion: HS biosynthesis is prioritized over CS biosynthesis. The balance between *extl3* and *csgalnact1/csgalnact2* function determines the HS/CS ratio.
Significance: Disease progression caused by HS deficiency may be affected by altered CS biosynthesis.

The present study addresses the roles of heparan sulfate (HS) proteoglycans and chondroitin sulfate (CS) proteoglycans in the development of zebrafish pharyngeal cartilage structures. *uxs1* and *b3gat3* mutants, predicted to have impaired biosynthesis of both HS and CS because of defective formation of the common proteoglycan linkage tetrasaccharide were analyzed along with *ext2* and *extl3* mutants, predicted to have defective HS polymerization. Notably, the effects on HS and CS biosynthesis in the respective mutant strains were shown to differ from what had been hypothesized. In *uxs1* and *b3gat3* mutant larvae, biosynthesis of CS was shown to be virtually abolished, whereas these mutants still were capable of synthesizing 50% of the HS produced in control larvae. *extl3* and *ext2* mutants on the other hand were shown to synthesize reduced amounts of hypersulfated HS. Further, *extl3* mutants produced higher levels of CS than control larvae, whereas morpholino-mediated suppression of *csgalnact1/csgalnact2* resulted in increased HS biosynthesis. Thus, the balance of the Extl3 and Csgalnact1/Csgalnact2 proteins influences the HS/CS ratio. A characterization of the pharyngeal cartilage element morphologies in the single mutant strains, as well as in *ext2;uxs1* double mutants, was conducted. A correlation between HS and CS production and phenotypes was found, such that impaired HS biosynthesis was shown to affect chondrocyte intercalation, whereas impaired CS biosynthesis inhibited formation of the extracellular matrix surrounding chondrocytes.

The pharyngeal apparatus is a vertebrate-specific structure that arises from all three germ layers. In zebrafish, the pharyngeal apparatus gives rise to the pharyngeal cartilage. One of the main functions of this cartilage is to provide mechanical support to the skeletal structures of the head and jaw. Pharyngeal cartilage formation begins as neural crest-derived prechondrocytic cells differentiate to chondrocytes and begin to secrete an extracellular matrix (ECM)[7] rich in collagen and proteoglycans (PGs) (1, 2). The early cartilage elements are then shaped in a process where the chondrocytes intercalate and flatten. This generates long and slender early cartilages elements that generally are one cell thick, somewhat similar to a stack of coins (3). The ability to make rod-like cartilages by intercalation of chondrocytes is conceivably ancient in vertebrates. These structures are present in both lamprey (4) and osteichthyans, showing that it is an ancestral vertebrate trait with a history probably extending back more than 500 million years. Direct evidence for its early existence comes from the 380-million-year-old fossil

* The work was supported by funds from the Swedish Research Council (to J. K., P. A., and J. L.), the Swedish Cancer Society (to J. K., D. S., and A. E.), the Swedish Childhood Cancer Foundation (to J. K.), Swedish Foundation for Strategic Research Project A3 05:207g (to J. K.), the Foundation for Proteoglycan Research at Uppsala University (J. K., D. S., A. E.), the Knut and Alice Wallenberg Foundation (J. L., P. A.), and the Linnaeus Framework Grant "Genomics of Phenotypic Diversity in Natural Populations" (J. L., P. A.).

[S] This article contains supplemental Tables S1 and S2, Figs. S1–S6, and Movies S1 and S2.

[1] These authors contributed equally to this work.

[2] Supported by the Danish National Research Foundation and The Dept. of Biomedical Sciences at The University of Copenhagen.

[3] Supported by Grant LSHC-CT-2006-018814 from the European Network of Excellence EuroBoNeT.

[4] These authors contributed equally to this work.

[5] To whom correspondence may be addressed: Dept. of Medical Biochemistry and Microbiology, Science for Life Laboratory, Uppsala University, Husargatan 3, P.O. Box 582, SE-751 23, Uppsala, Sweden. Tel.: 46-18-4714366; Fax: 46-18-4714673; E-mail: Johan.Kreuger@imbim.uu.se.

[6] To whom correspondence may be addressed: Dept. of Organism Biology, Science for Life Laboratory, Uppsala University, Norbyvägen 18A, SE-752 36 Uppsala, Sweden. Tel.: 46-18-4716120; Fax: 46-18-4712000; E-mail: Johan.Ledin@ebc.uu.se.

[7] The abbreviations used are: ECM, extracellular matrix; HS, heparan sulfate; CS, chondroitin sulfate; PG, proteoglycan; GAG, glycosaminoglycan; HexA, hexuronic acid; hpf, hours post fertilization; RPIP, reverse phase ion pair; dpf, days post fertilization; MO, morpholino; MHE, multiple hereditary exostoses; CSase, Chondroitinase.

Euphanerops, a jawless vertebrate possibly related to lamprey (5). Mineralized fragments of gill arch cartilages from this animal clearly show a cellular organization indistinguishable from that in modern examples, such as the zebrafish (supplemental Fig. S1). The mechanisms producing the characteristic cellular architecture of cartilages are thus likely to be both very old and of great importance for vertebrate morphogenesis in general.

An ECM, important for chondrogenesis and cartilage morphogenesis, is deposited between chondrocytes and the overlaying perichondrium (2). This ECM is rich in PGs carrying covalently attached glycosaminoglycan (GAG) polysaccharide side chains of heparan sulfate (HS) or chondroitin sulfate (CS) type. HS and CS differ with regard to the composition of the polysaccharide backbones, but HS and CS are similar in that they both have a high content of *O*-sulfate groups. These sulfate groups form clusters of negative charge along the GAG chains that mediate interactions with positively charged surfaces on protein ligands (6). Examples of signaling proteins relevant to cartilage and bone formation that interact with PGs include bone morphogenetic proteins, hedgehogs, Wnt signaling proteins, and fibroblast growth factors (7). PGs are abundantly expressed at the cell surface of most types of cells, including chondrocytes, and function as co-receptors. Others and we have shown that PGs shape the gradients of secreted morphogens during development to impact organ formation (8).

A number of genes involved in PG biosynthesis have been shown to be crucial for the development of the jaw and the pharyngeal arches in zebrafish, including *glypican 4* (*gpc4/knypek*) (9, 10), *UDP-glucuronic acid decarboxylase 1* (*uxs1*) (11, 12), *exostosin 2* (*ext2/dackel*) (12–15), *exostoses (multiple)-like 3* (*extl3/boxer*) (15), *udp-glucose dehydrogenase* (*ugdh/jekyll*) (16, 17), and *solute carrier family 35, member B2* (*slc35b2/pincher*, reported as *papst1*) (13). From previous studies of these genes, it stands relatively clear that PGs are required for the intercalation of chondrocytes during the formation of rod-like cartilage structures. For example, in *ext2* mutants suggested to synthesize only a fraction of normal HS levels (14), chondrocytes were found to be incapable of forming columns (13, 15). Interestingly, the *uxs1* gene has been suggested to be crucial for both HS and CS synthesis and shown by Eames *et al.* (11) to develop a cartilage phenotype similar to that found in *ext2* mutants, which would suggest that removal of CS in addition to the lack of HS would not result in a strengthened phenotype. From this it may be concluded that low HS content is the main reason for the abnormal cartilage development in both *ext2* and *uxs1* mutants. However, although *ext2* mutants also exhibit an almost complete absence of pectoral fin development, *uxs1* mutants were shown to develop only a mild pectoral fin phenotype (11, 14, 18). Because pectoral fin development is demonstrated to be dependent on HS (19), this would suggest that the block of HS biosynthesis is incomplete in *uxs1* mutants.

Here we present a systematic investigation to show both qualitatively and quantitatively how the biosynthesis of HS and CS is affected in *ext2*, *extl3*, *uxs1*, and *glucuronosyltransferase 1* (*b3gat3*) mutants. Of note, these transgenic lines are effectively partial loss of function mutants for HS and CS biosynthesis, because of enzyme redundancy and maternal contribution. Our analyses show that the relatively mild cartilage phenotype seen in *extl3* mutants can be explained by increased production of CS. It was hypothesized that there is an interplay between HS and CS biosynthesis, and this was confirmed using experiments with morpholinos targeting *chondroitin sulfate synthase 1* (*chsy1*) or the two *chondroitin sulfate N-acetyl-galactosaminyltransferase* (*csgalnact*) *1* and *2*. Further, analyses of *uxs1* and *b3gat3* mutants show that HS biosynthesis is prioritized over CS biosynthesis in a situation where the levels of PG linkage tetrasaccharides are reduced. Finally, *ext2;uxs1* double mutants with severely reduced capacity to produce both HS and CS were shown to develop a stronger cartilage phenotype when compared with the individual mutants.

EXPERIMENTAL PROCEDURES

Fish Stocks—Zebrafish embryos were obtained in natural crosses. The following mutant lines were used: $ext2^{tw25e}$ *and* $extl3^{Tm70G}$ (14) and $b3gat3^{hi307}$ and $uxs1^{hi954}$ (20). In addition, the wild-type lines Wik and Tubingen were used, as well as the transgenic line *Tg*(*fli1:EGFP*)*y1* (21). To be able to follow cartilage development by live imaging, all mutant lines were crossed with *Tg*(*fli1:EGFP*)*y1.* To obtain double mutants, the $ext2^{tw25e}$ allele was crossed into $uxs1^{hi954}$; *Tg*(*fli1:EGFP*)*y1* background, and homozygous double mutants were sorted by phenotype. Embryos were cultured in system water, with or without the addition of 0.003% 1-phenyl-2-thiourea (Sigma) to inhibit pigmentation and staged using hours post fertilization (hpf) (22). Homozygous mutants were identified based on phenotype. Prior to freezing or fixing, embryos were anesthetized in tricaine methanesulfonate (Sigma-Aldrich).

Confocal Imaging of Zebrafish—Cartilage and bone development was followed in zebrafish embryos and larvae using a Zeiss confocal laser scanning microscope 700 with an additional heating and CO_2 chamber. The fish were anesthetized and embedded in 1% soft agarose containing 1% tricaine and kept at 28 °C during all experiments. For visualization of bone development, the larvae were incubated in 0.3% alizarin red (Sigma-Aldrich) in system water for 12 h prior to live imaging. For time lapse analysis, the fish were followed for 50 h beginning at 55 hpf; z-stacks were captured every 20 min.

Genotyping—DNA extraction of larvae was carried out by incubating the larvae in 100 μl of 10 mM Tris, pH 8, 2 mM EDTA, and 0.2% Triton X-100 at 55 °C for 2 h, followed by 3 min at 96 °C. The PCR was initiated with a denaturation step at 94 °C for 3 min followed by amplification for 30 cycles (94 °C for 30 s, 50 °C for 40 s, and 72 °C for 45s) and an elongation step at 72 °C for 5 min. In each genotyping PCR, three primers were added for either *b3gat3* or *uxs1*, two flanking the retroviral insert and one within the insert. This resulted in a 165-bp fragment for the *b3gat3* mutant allele and 360 bp for the wild-type allele or a 175-bp fragment for the *uxs1* mutant allele and a 375-bp fragment for the wild-type allele. The primers used are: *b3gat3* forward, 5′-GCCGAGACTGAAGGAGACCCT-3′, and reverse, 5′-GCGGAAGTTGCTGGTAGTCCG-3′; *uxs1* forward, 5′-ACACACGGCATCGAACTCTTCTTTA-3′, and reverse, 5′-GCTGCAAGTCTAGAGTCATGTCG-3′; and primer in the retroviral insert 5′-GCTAGCTTGCCAAACCTACA-

GGT-3′.[8] PCR products were analyzed on a 1% agarose-gel. *ext2* mutants were identified based on their complete lack of pectoral fins (23).

Transmission Electron Microscopy—Zebrafish larvae were fixed in a mixture of 2% paraformaldehyde and 2.5% glutaraldehyde in 0.1 M PBS at 4 °C overnight, followed by three washing steps with PBS, for 10 min each. The larvae were postfixed in 1% OsO_4 for 30 min and washed three times with PBS for 15 min each. Dehydration was performed in a series of 20, 30, 50, 70, 80, 90, 96, and 100% (2×) ethanol and 100% (2×) aceton. The samples were infiltrated 1:1 aceton:resin overnight and then transferred to 100% resin and incubated overnight. The larvae were embedded in fresh resin and polymerized at 50 °C for 2 days. Thin sections were contrasted with uranyl acetate and lead citrate. Grids were observed in a Zeiss supra 35-VP field emission SEM, equipped with a scanning transmission electron microscope detector for transmission microscopy at an accelerating voltage 25 kV.

Structural Analysis of HS and CS by Reverse Phase Ion Pair (RPIP)-HPLC—HS and CS were isolated from zebrafish embryos and larvae, degraded into disaccharides by enzymatic cleavage, and detected in a HPLC-based system essentially following the protocol described earlier (24). In short, GAGs were isolated by proteolytic cleavage, nuclease treatment, and DEAE ion exchange chromatography. The purified GAGs were cleaved with chondroitinase ABC, and 10% of the sample was analyzed to identify CS disaccharide components. HS was purified from the GAG fraction by a second DEAE purification step followed by cleavage with heparin lyases I–III. The two generated samples of HS and CS disaccharides, respectively, were subjected to RPIP-HPLC analysis followed by post-column derivatization with cyanoacetamide and detection in a fluorescence detector, essentially as described (24). The identity and the amount of the disaccharides were established by comparing the samples with HS and CS disaccharide standards. At least four samples were run for each mutant/morphant with siblings from the same clutch as matching controls, with the exception of *ext2;uxs1* mutants, which were run in duplicate.

Alcian Blue Staining—Alcian blue staining was performed on 4- and 6-dpf larvae as described previously (17).

Morpholino Injections—Morpholino (MO) antisense oligomers MO1-*chsy1* and MO3-*chsy1* (25) were used. The embryos were injected at the one-cell stage with a combination of 0.25 pmol of MO1-*chsy1* and 1.28 pmol of MO3-*chsy3* and at 24 hpf collected for RPIP-HPLC analysis of HS and CS. The zebrafish *csgalnact1* (accession number XM_001333443) and *csgalnact2* (accession number NM_001126397) orthologs were identified by using human sequences for CSGALNACT1 (reference number AB071403) and CSGALNACT2 (reference number BC030268) for a comparative TBLASTN analysis against the zebrafish genome database. Morpholinos for zebrafish *csgalnact1* (5′-CACAACTGGCAACCTCAACAACAAG-3′) and *csgalnact2* (5′-GATCTTCACCAGCCACAGTTTTGCA-3′) MOs were designed against the respective translational start sites to knock down maternal and zygotic expression. The embryos were injected at the one-cell stage with a combination of 0.27 pmol of MO-*csgalnact1* and 0.27 pmol of MO-*csgalnact2* and at 30 hpf were collected for RPIP-HPLC analysis of HS and CS. All morpholinos were purchased from GeneTools (Philomath, OR). Injections were done using a Narishige IM-31 microinjector (Narishige, Tokyo, Japan).

Real Time Quantitative PCR Analysis of Differential Gene Expression—RNA was isolated from pools of ~20 zebrafish embryos at 6 dpf using the miRNeasy mini kit (Qiagen). cDNA was synthesized using the iScript cDNA synthesis kit (Bio-Rad). Quantitative RT-PCRs were carried out using the SsoFast EvaGreen supermix (Bio-Rad). Amplification efficiency was determined using dilution series of the templates. Primer specificity was confirmed by melt-curve analysis and agarose gel analysis. All primer pairs used are shown in supplemental Table S1. Calculation of relative gene expression was performed using the $2 - \Delta\Delta C_T$ method (reference gene *rpl13a*) and normalization of the data to average gene expression levels in wild-type embryos. The *p* values for differential gene expression in *extl3* mutants *versus* wild type were calculated using the unpaired two-tailed Student's *t* test.

Size Analysis of GAGs Isolated from Zebrafish Embryos—Embryos were injected in the yolk with radioactive sulfate (^{35}S) at 5 dpf and harvested after 18 h, after which GAGs were isolated by protease and benzonase digestions, followed by DEAE (GE Healthcare) anion exchange chromatography, essentially as described previously (24). Purified GAGs were alkaline treated at a final concentration of 0.5 M NaOH for 16 h at 4 °C, and an aliquot of the reaction mixture was analyzed on Superose 6 (GE Healthcare Biosciences). The rest of the sample was subjected to either CSase ABC treatment (50 milliunits/sample), nitrous acid treatment at pH 1.5, or a combination of both these treatments prior to size analysis on a Superose 6 column followed by ^{35}S analysis by liquid scintillation counting.

Structural Analysis of GAG Chains Attached to AAS Syndecan-4—Transfections of HEK293 cells with an expression construct for HA-tagged AAS syndecan-4 (26) having only a single GAG attachment site, with or without co-transfection with *EXTL3* siRNA (Invitrogen; identification number 116968) were carried out using Ingenio transfection solution (Mirus Bio LLC) on a nucleofector device (Amaxa Inc.). 24 h post-transfection, the cells were labeled with 50 μCi/ml [^{3}H]glucosamine (PerkinElmer Life Sciences; specific activity, 37 Ci/mmol) for 24 h and harvested, and cell lysis was performed. HA-tagged AAS syndecan-4 was isolated using immunoprecipitation using a specific anti-HA antibody (H9658; Sigma) coupled to Dynabeads Protein G (Invitrogen), according to the manufacturer's instructions. The GAG chains were isolated as described above, and part of the samples were digested with either CSase ABC (50 milliunits/sample), nitrous acid treatment at pH 1.5, or a combination of both treatments prior to size separation on a Superose 12 column (GE Healthcare) followed by ^{3}H analysis by liquid scintillation counting.

RESULTS

Analysis of Zebrafish Cartilage Development by Live Imaging of EGFP-expressing Chondrocytes—To study the roles of HS and CS in pharyngeal development, we performed a systematic

[8] A. Amsterdam, personal communication.

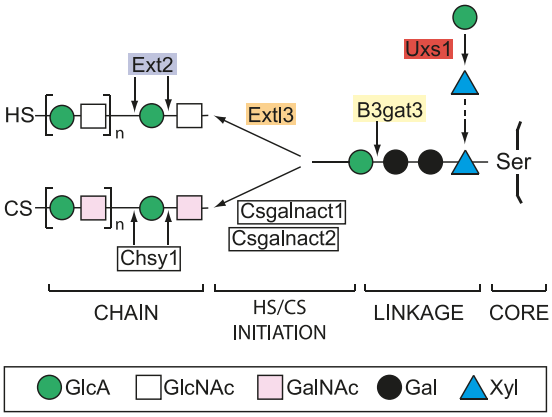

FIGURE 1. **Biosynthesis of GAGs.** The biosynthesis of HS and CS is initiated by the formation of a common PG tetrasaccharide linkage region. The first hexosamine added commits the intermediate to either HS or CS. The cartoon depicts key enzymatic reactions in the biosynthesis of HS and CS analyzed in the present study. Acronyms for genes whose functions are studied in zebrafish mutants are shown in *colored boxes*, and acronyms for genes whose functions are investigated by morpholino injections are shown in *framed boxes*.

comparison of pharyngeal defects in fish having mutations in enzymes of the GAG biosynthetic pathway. *ext2* and *extl3* mutants, defective in enzymes directly involved in HS polymerization, were analyzed together with *uxs1* and *b3gat3* mutants, predicted to have defective formation of the PG tetrasaccharide linkage region, presumably with consequences for both HS and CS biosynthesis (Fig. 1) (11, 14, 20). All of the investigated enzymes are ubiquitously expressed during zebrafish development (11, 14) (supplemental Fig. S2). We initially crossed all mutant alleles into the *fli:EGFP* genetic background to enable time lapse imaging using confocal microscopy of developing cartilages, because chondrocytes in this transgenic line have been shown to express GFP (21).

The organization of chondrocytes into cartilage elements normally begins at ~50 hpf. We initially followed the development of the pharyngeal cartilage in *fli:EGFP* transgenic embryos (here referred to as control) between 55 and 102 hpf by confocal microscopy. Chondrocytes in the pharyngeal cartilage elements were shown to adopt an elongated shape and to orient themselves perpendicular to the longitudinal axis of respective cartilage elements at ~60 hpf. Subsequently, intercalation occurred to produce elements where most cartilage cells span from one side of the perichondrium to the other (Fig. 2, *A* and *F*, and supplemental Movie S1) (3).

Chondrocytes in ext2 Mutants Remain Immobile during Initial Cartilage Organization—In *ext2* mutants, the chondrocytes have previously been shown to be incapable of proper intercalation (13, 15). Time lapse analysis of *ext2* mutants revealed that the formation of the Meckel's cartilage appeared normal until 65 hpf. Thereafter, chondrocytes in *ext2* mutants gradually stopped moving to finally become immobile (supplemental Movie S2). Notably, other complex morphogenetic processes in *ext2* mutants, such as the formation of the heart and blood vessels, apparently proceeded in a normal fashion during the same time period (supplemental Movies S1 and S2). These results underline that chondrocyte organization and cartilage morphogenesis is particularly sensitive to a reduction of *ext2* function.

uxs1 and b3gat3 Mutants Exhibit Abnormal Pharyngeal Cartilage Morphogenesis—The pharyngeal cartilage elements of *ext2*, *uxs1*, and *b3gat3* mutants were shown to be shorter and thicker than those of control larvae (Fig. 2). Rearrangement and proper intercalation of chondrocytes rarely occurred in these mutants, resulting in short and thick cartilage elements. The defects in chondrocyte intercalation affected the overall development of the jaw region, which was compressed along the anterior-posterior axis to a similar extent in *ext2*, *uxs1*, and *b3gat3* mutants (Fig. 2, *P* and *R–T*).

Chondrocytes Intercalate in extl3 Mutants—To better understand the effects of defective HS and CS biosynthesis in pharyngeal cartilage development, we extended our analysis to include *extl3* mutants (Fig. 1). *extl3* mutants have previously been shown to synthesize slightly more HS than *ext2* mutants (14), whereas the *extl3* mutant pectoral fin phenotype is similar (Fig. 2*L*) compared with *uxs1* and *b3gat3* mutants (Fig. 2, *N* and *O*). However, in comparison with *ext2*, *uxs1*, and *b3gat3* mutants, *extl3* mutants develop significantly milder pharyngeal cartilage phenotypes. Accordingly, many chondrocytes in the Meckel's cartilage and the ceratohyal cartilage were shown to be flattened and oriented perpendicular to the length of the arch elements (Fig. 2, *B* and *G*) (15). *extl3* mutants are thus in part able to organize chondrocytes similar to wild type (Fig. 2, *A* and *F*), although the organization of chondrocytes into single-cell rods often is incomplete (Fig. 2*G*). The milder cartilage phenotype in *extl3* mutants was also manifested by a significantly more efficient extension of the pharyngeal cartilages along the anterior-posterior axis (Fig. 2*Q*) compared with the other mutant strains (Fig. 2, *R–T*), but the *extl3* mutants still exhibited slightly shorter and thicker cartilages as compared with control larvae (Fig. 2*P*). The *extl3* mutant pharyngeal cartilage phenotype is thus a mild version of the phenotypes observed in *ext2*, *uxs1*, and *b3gat3* mutants, whereas paradoxically the pectoral fin phenotype is similar in *extl3*, *uxs1*, and *b3gat3* mutants (Fig. 2, *K–O*). It could be assumed that mutations in *ext2* and *extl3* would result in defective HS biosynthesis but have no effect on CS biosynthesis. Mutations in *uxs1* and *b3gat3* mutants would, on the other hand, be expected to have defective or even absent biosynthesis of both HS and CS (Fig. 1). The comparison of the pharyngeal cartilage and the pectoral fin phenotypes in *extl3*, *ext2*, *uxs1*, and *b3gat3* mutants, however, suggested that this assumption is an oversimplification and that mutations in these enzymes may have other effects on HS and CS biosynthesis than predicted based on their respective positions in the GAG biosynthetic pathway.

HS Content Correlates to the Pectoral Fin Phenotype—To be able to correlate the observed morphological phenotypes with the actual effects on GAG biosynthesis, we performed a detailed quantitative comparison of HS and CS biosynthesis in all the mutants. Offspring from crossings of heterozygous mutant strains were based on gross mutant morphology sorted into two pools: mutant larvae and unaffected siblings (control). Total GAGs from wild-type fish as well as from the above described crosses of the mutant lines were isolated at 6 dpf and analyzed by RPIP-HPLC analysis (see "Experimental Procedures"). This method has the advantage of allowing the determination of both the total HS and CS content, as well as the

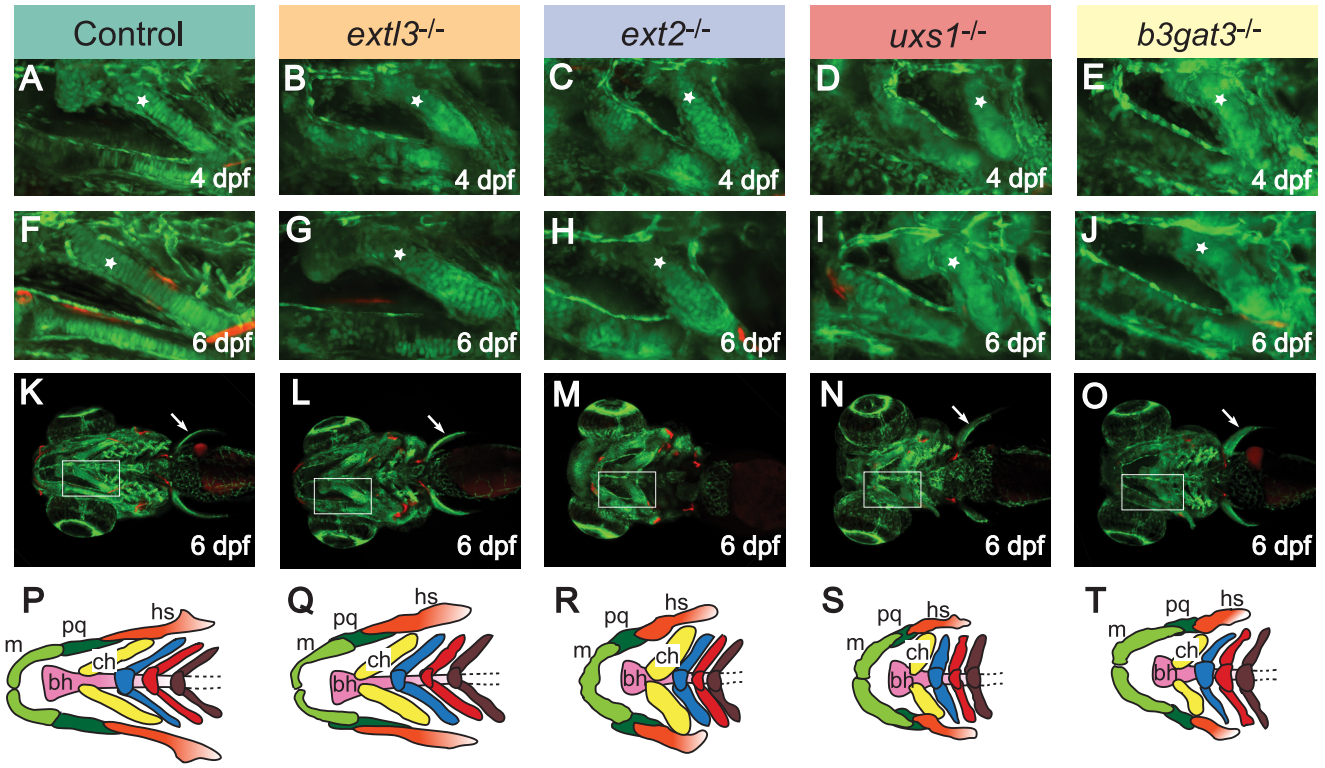

FIGURE 2. ***extl3* mutants have a milder cartilage phenotype compared with *ext2*, *uxs1*, and *b3gat3* mutants.** Ventral views of pharyngeal cartilage elements of *fli1:EGFP* zebrafish larvae at 4 and 6 dpf. In wild-type larvae (*A*, *F*, and *K*), chondrocytes intercalate and elongate to form ordered parallel stacks resulting in slender cartilage structures. In contrast, fish homozygous for mutations in the GAG biosynthetic enzymes *extl3* (*B*, *G*, and *L*), *ext2* (*C*, *H*, and *M*), *uxs1* (*D*, *I*, and *N*), and *b3gat3* (*E*, *J*, and *O*) all exhibit abnormal cartilage formation. *ext2*, *uxs1*, and *b3gat3* mutants display the strongest phenotypes with abnormally short and disorganized cartilage structures, where mutant chondrocytes generally appear round and do not display complete intercalation. The *exl3* mutant cartilage phenotype is markedly milder. The *rectangles* in *K*–*O* indicate magnified areas shown in *A*–*J*. The areas where bone is forming are stained with alizarin red. *P*–*T* show schematic drawings of cartilage structures in the first five pharyngeal arches. *bh*, basihyal; *ch*, ceratohyal; *hs*, hyosymplectic; *m*, Meckel's cartilage; *pq*, palatoquadrate.

relative occurrence of the different modified (sulfated) disaccharide species present in respective GAG pools (24). We found that *extl3* mutants have a higher HS content (44% of control) than *ext2* mutants (17% of control) at 6 dpf, in line with previously reported results (14). Surprisingly however, *uxs1* and *b3gat3* mutants were shown to contain half of the normal HS content (52 and 55% of control, respectively) (Fig. 3*A*). Thus, the severity of the pectoral fin phenotype, but not the pharyngeal cartilage phenotype, was shown to correlate to the HS content in the different mutant larvae.

The Level of CS Biosynthesis Correlates to the Cartilage Phenotypes—Analysis of the CS content at 6 dpf made it possible to address the hypothesis that the combined amounts of HS and CS might correlate to the pharyngeal cartilage mutant phenotypes. Surprisingly, *uxs1* and *b3gat3* mutants were shown to have very low levels of CS (5 and 11%, respectively, of control). Thus, the inability to efficiently form the PG tetrasaccharide linkage region in these mutants resulted in a much more dramatic reduction of CS biosynthesis as compared with HS biosynthesis (Fig. 3*A*). CS biosynthesis in *ext2* mutants was, in contrast, similar to the wild type (88% of control). Interestingly, *extl3* mutants were shown to produce more CS than control larvae (147% of control) (Fig. 3*A*), indicating that reduced HS initiation leading to an increased CS accumulation could explain the mild cartilage phenotypes observed in these mutants (Fig. 2, *B*, *G*, *L*, and *Q*).

The Balance between extl3 and csgalnact1/csgalnact2 Influences the HS/CS Ratio—Based on the molecular phenotypes of the *extl3* larvae, we hypothesized that the balance between *extl3* and *csgalnact1/csgalnact2* expression impacts the HS/CS ratio (Fig. 1). We also hypothesized that blunting the activity of *chsy1* to suppress CS polymerization would not impact HS biosynthesis, analogous to the finding in *ext2* mutants, where HS biosynthesis, but not CS biosynthesis, was shown to be suppressed (Fig. 3*A*). To this end, morpholino injections of wild-type embryos to target *chsy1* (27) or *csgalnact1/csgalnact2* were performed. Morpholinos targeting *chsy1* indeed resulted in a 50% decrease of CS production, whereas there was no effect on HS biosynthesis (Fig. 3*B*). In contrast, injection of a mixture of morpholinos to suppress the CS initiation enzymes Csgalnact1 (28, 29) and Csgalnact2 (29, 30) decreased CS accumulation and increased HS accumulation (Fig. 3*C*).

We next investigated whether a decrease in *extl3* expression could affect the HS/CS substitution ratio on a specific proteoglycan core protein. HA-tagged AAS Syndecan-4 containing only a single GAG attachment site (26) was expressed in HEK cells treated with *extl3*-siRNA leading to reduction of the *extl3* mRNA levels by ~60% (data not shown). HA-tagged AAS Syndecan-4 was thereafter isolated by immunoprecipitation (supplemental Fig. S6). Interestingly, blunting of *extl3* expression was shown to reduce the HS/CS ratio, so that AAS Syndecan-4 carried a larger proportion of CSase-sensitive material in

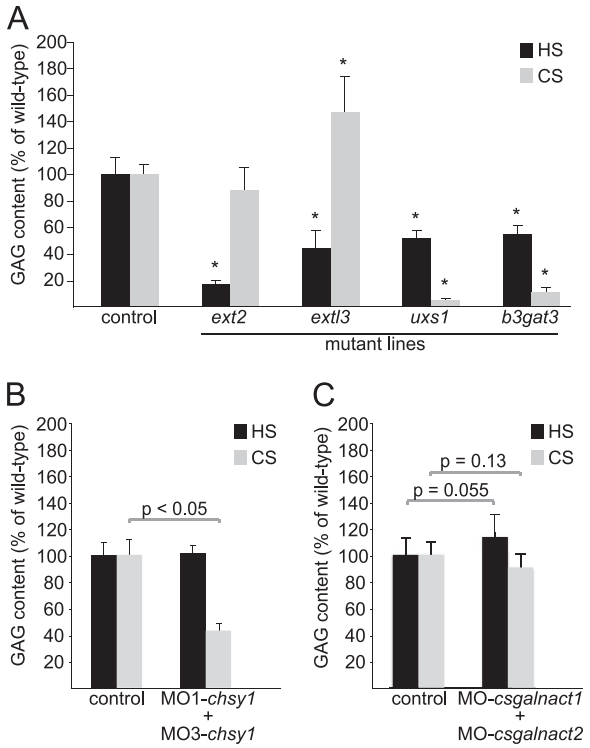

FIGURE 3. **In addition to reduced HS biosynthesis, *uxs1* and *b3gat3* mutant larvae exhibit severely reduced CS biosynthesis, whereas *extl3* mutants have increased CS production.** HS and CS were quantitatively isolated from the various zebrafish strains at 6 dpf and analyzed using RPIP-HPLC, as described previously (24). *A*, the amounts of HS and CS (pmol/larvae) in the mutant lines are shown as percentages of the levels found in sibling controls (set to 100%). Whereas all enzyme mutants show a reduced production of HS (17–55% of wild type), the different mutant strains differ greatly in their production of CS. *B* and *C*, the amounts of HS and CS (pmol/larvae) in zebrafish larvae at 6 dpf injected with morpholinos targeting *chsy1* (*B*) or *csgalnact1* and *csgalnact2* mRNA (*C*), here shown as percentages of the levels found in sibling controls (set to 100%). Whereas suppression of *chsy1* only reduces CS production, suppression of *csgalnact1* and *csgalnact2* results in reduced CS production together with increased HS production. The *asterisks* illustrate a significant difference in disaccharide content as compared with sibling controls ($p < 0.05$).

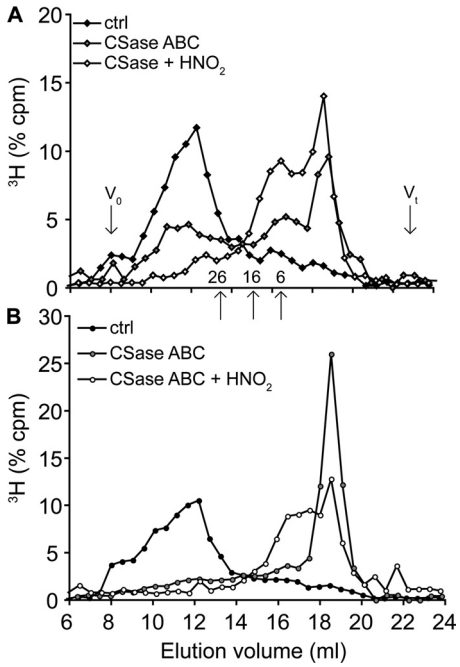

FIGURE 4. **Suppression of *extl3* results in increased relative levels of CS attached to AAS syndecan-4.** HA-tagged AAS syndecan-4 was expressed in HEK293 cells transfected with siRNA control (*A*) or siRNA targeting *extl3* (*B*). AAS syndecan-4 was further isolated by immunoprecipitation, and GAG attached to the core protein isolated and analyzed by gel filtration on a Superose 12 column. *A*, in the control condition, the intact GAGs (*filled diamonds*) eluted mainly as a single broad peak. CSase ABC digestion (*gray diamonds*) together with combined CSase ABC and nitrous acid treatment at pH 1.5 (*open diamonds*) showed that ~30% of the high molecular weight GAG chains were of CS type. *B*, in the *extl3*-siRNA condition, the AAS syndecan-4 GAGs similarly eluted as a broad peak (*filled circles*). CSase ABC digestion (*gray circles*) together with combined CSase ABC and nitrous acid treatment at pH 1.5 (*open circles*) showed that ~ 65% of the GAG chains were of CS type. The elution positions of 6-, 16-, and 26-mer dextran saccharide standards are shown. *ctrl*, control.

siRNA-treated cells compared with control cells (Fig. 4). This illustrates that reduced Extl3 function can decrease the HS/CS ratio on a specific core protein at the level of a single GAG attachment site. Taken together, our data suggest that the balance between *extl3* and *csgalnact1/csgalnact2* expression affects the HS/CS ratio, possibly by a mechanism where there is competition or altered usage of available GAG linkage regions.

To test whether the increased accumulation of CS in *extl3* mutants (Fig. 3*A*) contributed to the relatively mild cartilage phenotype seen here as compared with *ext2* mutant larvae, morpholinos targeting *chsy1* were injected in *extl3* mutants. It was found that a decrease in CS synthesis in the *extl3* morphants resulted in a stronger phenotype exhibiting compressed jaws with shorter and thicker cartilage elements (supplemental Fig. S5).

Differential Core Protein Expression, but Not Changes in CS Chain Length, May Contribute to Increased CS Content in extl3 Mutants—Cell culture experiments have previously shown that the length of GAG chains can be altered as a result of suppressed expression of GAG biosynthetic enzymes (31). To investigate whether the increased CS content in *extl3* mutants could be explained by the formation of longer CS chains, we injected 5 dpf embryos with radioactive sulfate and isolated ^{35}S-labeled GAGs at 18 h post-injection. A majority of the isolated total GAG chains were of CS type and susceptible to CSase cleavage (Fig. 5*A* and supplemental Table S2). The isolated GAG pools were also subjected to nitrous acid treatment that specifically degrades HS. It was concluded that the intact CS chain populations from both wild type and *extl3* mutants had the same size distributions (Fig. 5*B*).

Another possible mechanism for the increased CS content in *extl3* mutants could possibly be altered expression of core proteins or glycosyltransferases involved in GAG polymerization. To this end, we quantified the expression of a number of genes directly involved in proteoglycan biosynthesis using a quantitative PCR approach. The expression levels of most investigated genes were similar in *extl3* mutants and control embryos at 6 dpf (Fig. 6). Only the biglycan (*bgna*) mRNA level was significantly reduced in *extl3* mutant embryos. However, a tendency for elevated aggrecan (*acana*) mRNA was seen in *extl3* mutants (1.6-fold difference *versus* wild-type control; $p = 0.25$).

ext2 and extl3 Are Required for Normal HS Sulfation—Disaccharide analysis of HS produced by the mutant strains revealed that the proportion of sulfated disaccharides was increased in both *ext2* and *extl3* mutants. The prevalence of the disaccharide

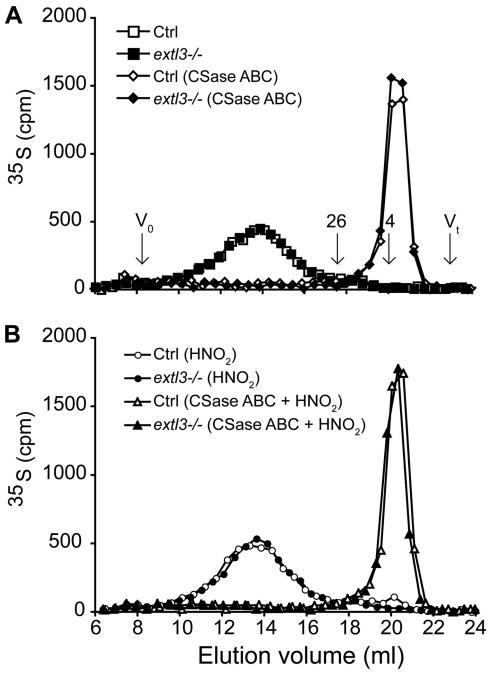

FIGURE 5. **Increased CS content in *extl3* mutants does not correlate to increased CS chain length.** GAGs isolated from *extl3* mutants and sibling controls were analyzed by gel filtration on a Superose 6 column. *A*, GAGs from the *extl3* mutants (*filled squares*) and their siblings (*open squares*) exhibited identical elution profiles indicating no or very small differences in chain length. Treatment with CSase ABC cleaved most of the material both in *extl3* mutants (*filled diamonds*) and siblings (*open diamonds*). *B*, nitrous acid treatment at pH 1.5 in addition degraded HS present in the total GAG pool isolated from *extl3* mutants (*filled circles*) and siblings (*open circles*). Digestions with both CSase ABC and nitrous acid at pH 1.5 cleaved nearly all of the isolated material in both *extl3* mutants (*filled triangles*) and siblings (*open triangles*). The elution positions of 4- and 26-mer dextran saccharide standards are indicated (see supplemental Table S2 for a quantification of the results). *Ctrl*, control.

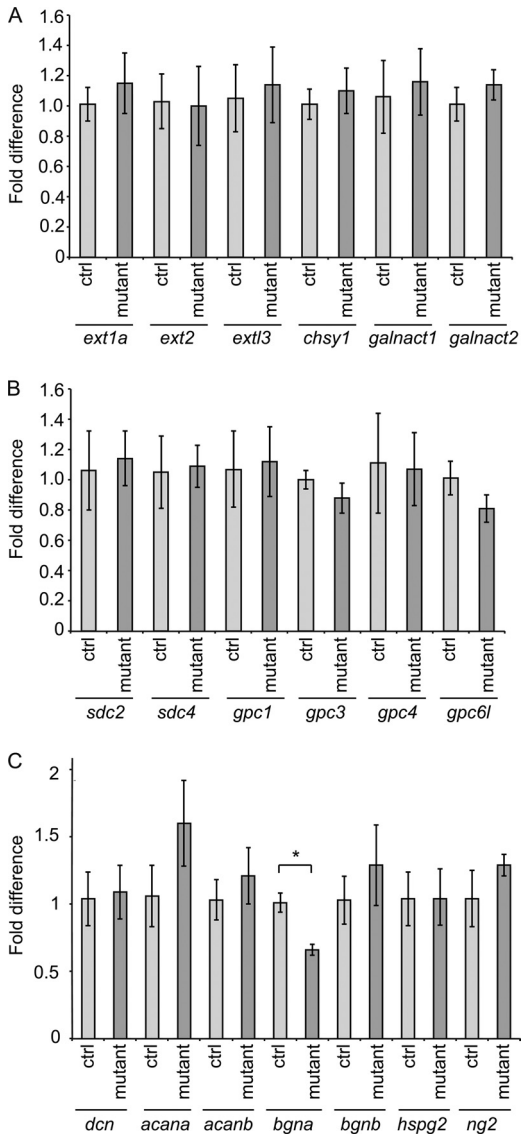

FIGURE 6. **The expression levels of genes coding for proteoglycan core proteins and enzymes involved in polymerization of HS and CS are relatively unaffected in *extl3* mutants.** Real time quantitative PCR analysis was performed to evaluate the expression levels of selected genes *extl3* mutant larvae compared with wild-type larvae isolated at 6 dpf ($n = 3$). The relative expression of genes coding for glycosyltransferases involved in HS and CS polymerization (*A*), membrane-tethered proteoglycan core proteins (*B*), or secreted proteoglycan core proteins (*C*) are shown. *ctrl*, control.

species devoid of sulfate groups (ΔHexA-GlcNAc) was decreased by 34% in *ext2* mutants and 42% in *extl3* mutants (Fig. 4), whereas the proportion of disaccharides modified by 6-*O*-sulfate groups was increased by 69 and 51%, respectively, in these mutants (supplemental Fig. S3*A*). The main consequence of the increased 6-*O*-sulfation was the increased occurrence of the ΔHexA2S-GlcNS6S disaccharide, commonly found in HS domains interacting with proteins, and a corresponding decrease in ΔHexA2S-GlcNS (Fig. 7). Interestingly, *uxs1* and *b3gat3* mutants displayed the opposite tendency with a decreased occurrence of ΔHexA2S-GlcNS6S and an increase of ΔHexA2S-GlcNS (Fig. 7).

uxs1 and b3gat3 Mutants Are Incapable of CS 6-O-Sulfation—Despite the reduced and abnormal HS biosynthesis in *ext2* and *extl3* mutants, the level of CS sulfation in these mutants was found to be similar compared with control larvae (Fig. 8). In contrast, *uxs1* and *b3gat3* mutants produced very low amounts of CS with a striking reduction of ΔHexA-GalNAc6S disaccharide content accompanied by an increased content of ΔHexA-GalNAc4S disaccharides (Fig. 8).

ext2;uxs1 Double Mutants Have Stronger Cartilage Phenotypes than the Respective Single Mutants—Double mutants were created by introducing the *ext2* mutant allele into the background of *uxs1*;*Tg*(*fli:EGFP*). The double mutants thus combine the *ext2* genotype showing the strongest reduction of HS synthesis (18% of control) with the *uxs1* genotype displaying the strongest reduction in CS synthesis (5% of control) (Fig. 3), to test the hypothesis that a strong suppression of both HS and CS biosynthesis simultaneously should lead to stronger phenotypes. To confirm that both HS and CS synthesis were suppressed in the *ext2;uxs1* double mutants, we analyzed for GAG content of these larvae at 4 dpf; later stages were not amendable to analysis because of increased mortality. The HS content was shown to be reduced to 13% of control, and the CS content was reduced to 16% of control (Fig. 9*A*). The HS sulfation pattern in the double mutants was similar to that of *ext2* and *extl3* single mutants, with an increase in ΔHexA2S-GlcNS6S, but with the difference that there was a smaller reduction of ΔHexA2S-GlcNAc (Fig. 9*B*). The CS composition was shown

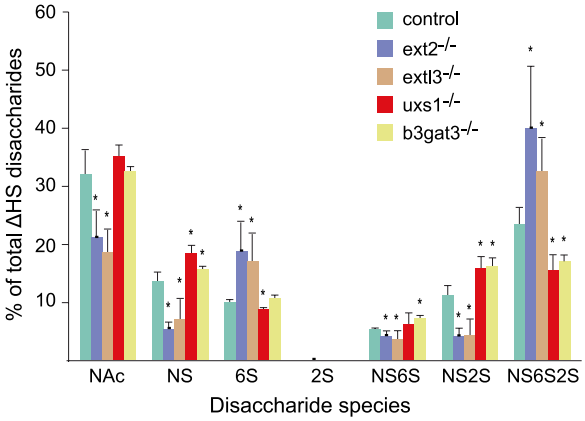

FIGURE 7. ***extl3* and *ext2* mutant larvae produce hypersulfated HS.** The HS disaccharide profiles of all the mutant strains together with wild-type zebrafish larvae at 6 dpf are shown. Whereas *extl3* and *ext2* mutants produce an oversulfated HS, *uxs1* and *b3gat3* mutants essentially produce a wild-type HS with regard to overall degree of sulfation and disaccharide composition. The relative proportion of all disaccharides was determined for each sample. Disaccharide species are indicated as NAc (ΔHexA-GlcNAc), NS (ΔHexA-GlcNS), 6S (ΔHexA-GlcNAc6S), 2S (ΔHexA2S-GlcNAc), NS6S (ΔHexA-GlcNS6S), NS2S (ΔHexA2S-GlcNS), and NS6S2S (ΔHexA2S-GlcNS6S). The *asterisks* illustrate a significant difference in disaccharide content as compared with siblings ($p < 0.05$).

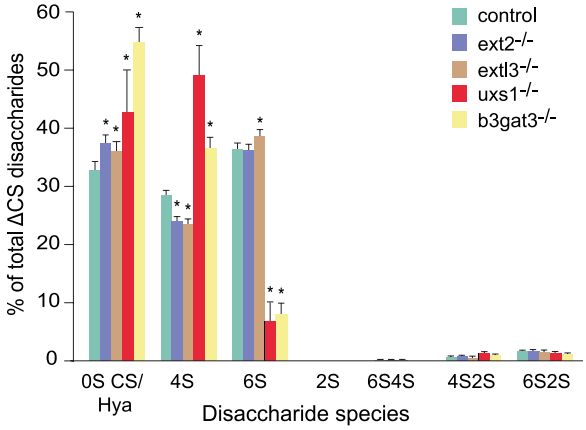

FIGURE 8. ***uxs1* and *b3gat3* mutant larvae produce undersulfated CS with reduced 6-*O*-sulfate content but with increased 4-*O*-sulfate content.** The CS disaccharide profiles of the mutant strains together with wild-type zebrafish at 6 dpf are shown. *extl3* and *ext2* mutants produce a CS that is similar to that of wild type and *uxs1* and *b3gat3* mutants produce a CS with almost no 6-*O*-sulfate content but with up to a 2-fold increase of the 4-*O*-sulfate content. The relative proportion of each disaccharide was determined for each sample. Disaccharide species are indicated as *0S CS/Hya* (ΔHexA-GalNAc/ΔHexA-GlcNAc), *4S* (ΔHexA-GalNAc4S), *6S* (ΔHexA-GalNAc6S), *2S* (ΔHexA2S-GalNAc), *6S4S* (ΔHexA-GlcNAc4S6S), *4S2S* (ΔHexA2S-GalNAc4S), and *6S2S* (ΔHexA2S-GalNAc6S). The *asterisks* illustrate a significant difference in disaccharide content as compared with siblings ($p < 0.05$).

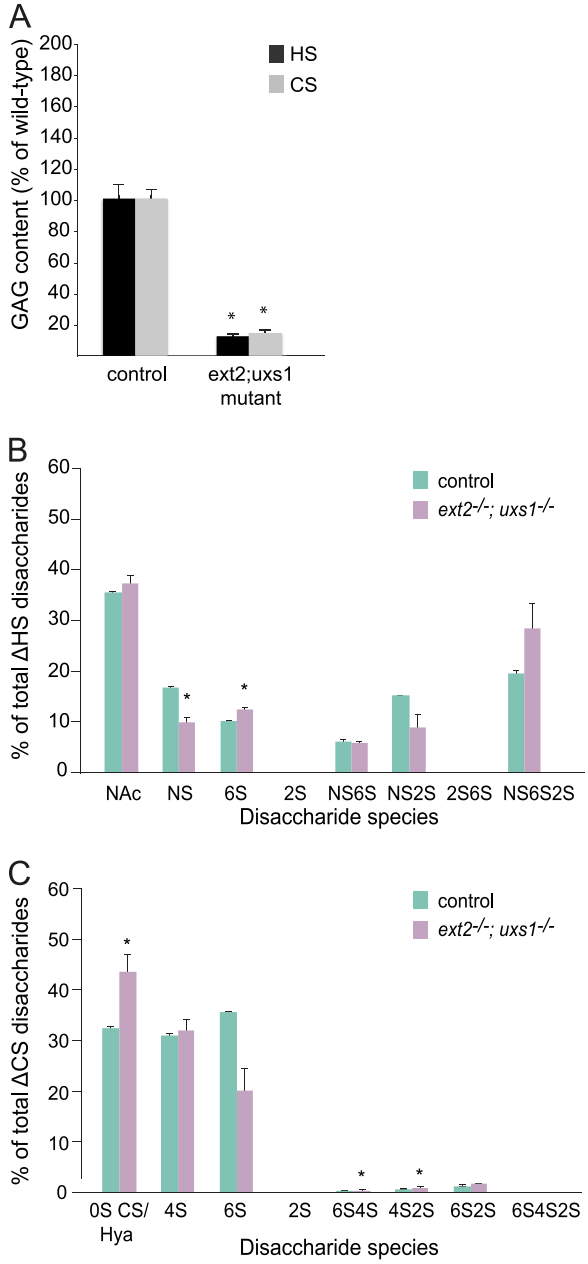

FIGURE 9. ***ext2;uxs1* double mutant larvae have severely reduced production of both HS and CS.** *A*, HS and CS were quantitatively isolated from double mutants at 4 dpf (later stages were not amendable to analysis because of lethality) and analyzed using RPIP-HPLC. The amounts of HS and CS (pmol/larvae) in the mutant lines are shown as percentages of the levels found in sibling controls (set to 100%). *B* and *C*, the HS disaccharide profiles (*B*) and CS disaccharide profiles (*C*) of *ext2;uxs1* double mutants compared with control zebrafish larvae at 4 dpf. The results show increase 6-*O*-sulfation of HS accompanied by decreased 6-*O*-sulfation of CS in the double mutants ($p < 0.05$).

to be similar to that of *uxs1* and *b3gat3* single mutants with a decrease in ΔHexA-GalNAc6S, but with the difference that there was less ΔHexA-GalNAc4S (Fig. 9*C*).

The *ext2;uxs1* double mutants were further shown to develop pharyngeal cartilage phenotypes that in a direct comparison were significantly stronger compared with the phenotypes found in the single *ext2* and *uxs1* mutants. Coherent groups of *EGFP* positive cells belonging to the pharyngeal arches were, however, identified in the double mutants (Fig. 10, *D* and *H*), indicating that low levels of HS and CS are tolerable for precartilage condensation. However, the pharyngeal cartilages were very small and severely misshaped at 4 dpf, and the anterior-posterior extension of the pharyngeal cartilage was also reduced compared with the control, as well as compared with the single mutants (Fig. 10).

To study how different amounts of HS and CS affect cartilage development, we imaged the ultrastructure of the ceratohyal elements in larvae at 4 dpf using transmission electron microscopy. The chondrocytes in the control were shown to be fully intercalated and embedded in a thick layer of ECM (Fig. 10*I*). *ext2* mutant chondrocytes, on the other hand, clearly failed to elongate and did not intercalate properly but were able to pro-

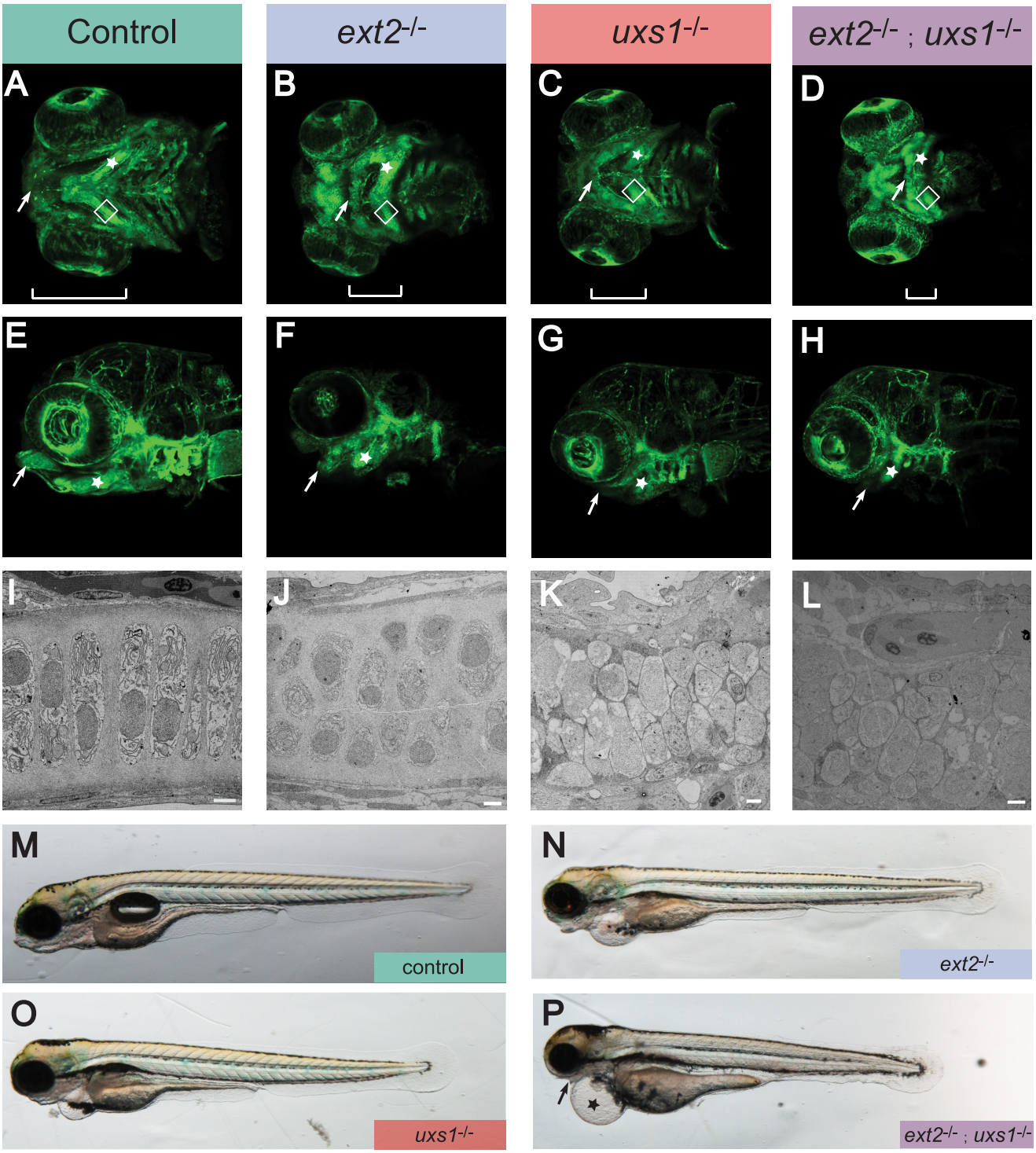

FIGURE 10. **Impaired HS biosynthesis leads to aberrant chondrocyte intercalation, and impaired CS biosynthesis inhibits ECM formation.** Confocal imaging of live *fli1:EGFP* zebrafish larvae at 4 dpf. Shown are ventral views (*A–D*) and lateral views (*E–H*) of pharyngeal cartilage elements. *A* and *E*, control; *B* and *F*, *ext2* mutants; *C* and *G*, *uxs1* mutants; *D* and H, *ext2;uxs1* double mutants. The lengths of the Meckel's cartilage (*arrows* in *A–H*) and the ceratohyal cartilage (*stars* in *A–H*) are significantly shorter in *ext2;uxs1* double mutants compared with the *ext2* and *uxs1* mutants. The distance between the anterior end of Meckel's cartilage and the posterior end of the ceratohyal is indicated by brackets in *A–D*. Note that this distance is reduced in both *ext2* and *uxs1* mutants compared with control larvae and also strongly reduced in *ext2;uxs1* double mutants. *I–L* show transmission electron microscopy images of the ceratohyal elements at 4 dpf. The *rectangles* in *A–D* serve to indicate the regions magnified in *I–L*. *I*, in control larvae, the chondrocytes are elongated and organized in rows surrounded by a thick layer of ECM. *J–L*, chondrocytes in *ext2* mutants (*J*) are round and disorganized but still synthesize large amounts of ECM, whereas chondrocytes in *uxs1* mutants (*K*) are tightly packed together and very little ECM can be detected (*L*). *ext2;uxs1* double mutants produce lower amounts of ECM compared with *uxs* mutants, and most of the chondrocytes have neither elongated nor intercalated properly. *Scale bars*, 3 μm. *M–P*, lateral brightfield views of zebrafish larvae at 4 dpf. *ext2;uxs1* double mutants (*P*) display a more severe jaw phenotype (*arrow* in *P*) compared with *ext2* (*N*) and *uxs1* (*O*) mutants. The double mutants also frequently develop a distinct pericardial edema (*star* in *P*) surrounding the heart, as well as exhibiting reduced eye size.

duce large amounts of ECM (Fig. 10*J*). Chondrocytes in *uxs1* mutants also did not intercalate properly and in addition produced low levels of electron-dense ECM (Fig. 10*K*). Further, chondrocytes in *ext2;uxs1* double mutants produced even less ECM than the *uxs1* mutants, and, in addition, very few cells adopted an elongated shape (Fig. 10*L*). Taken together, these results suggest that the capacity to produce HS is required for proper chondrocyte intercalation, whereas reduced CS biosynthesis leads to impaired production of the ECM. The ceratohyal ECM of *ext2* mutants was also shown to contain an organized collagen network, whereas only a few collagen fibers were observed in *uxs1* mutants. Notably, no collagen fibers could be detected in *ext2;uxs1* double mutants (supplemental Fig. S4).

Finally, analyses of the gross morphology showed that *ext2; uxs1* double mutants displayed a more severe jaw phenotype compared with *ext2* and *uxs1* mutants, respectively. In addition, the double mutants also often showed pericardial edema and reduced eye size.

DISCUSSION

In this study we show that HS and CS biosynthesis in zebrafish larvae homozygous for mutations in either *ext2*, *extl3*, *uxs1*, or *b3gat3* differs significantly from what could be hypothesized based on the results of previous studies and from the proposed positions of these enzymes in the GAG biosynthetic pathway (Fig. 1). Our study reveals that *ext2* mutants contain less than half of the HS content of *uxs1* and *b3gat3* mutants. This provides an explanation for the fact that the *uxs1* and *b3gat3* pectoral fin phenotypes are weaker than the *ext2* fin phenotype, because HS has been suggested to be critical for pectoral fin development (19). The present study also shows that *extl3* mutants have milder cartilage phenotypes than *ext2*, *uxs1*, and *b3gat3* mutants. This can be explained by the finding that *extl3* mutants have increased CS biosynthesis (147% of control). The *extl3* mutants therefore not only represent a HS loss of function model but also effectively represent a CS gain of function model. To our knowledge, this is the first time that a mutation in a GAG biosynthetic enzyme has resulted in quantitative up-regulation of CS biosynthesis *in vivo*. Finally, *ext2; uxs1* double mutants, generated from the two single mutant strains with the most dramatic reduction in HS and CS, respectively, were shown to develop a significantly stronger pharyngeal cartilage phenotype compared with the individual single mutant strains (Fig. 10), confirming the key roles of both HS and CS in cartilage formation and demonstrating an additive effect of these mutations. It should be noted that the RPIP-HPLC analysis used here provides information on the structure and absolute levels of HS and CS, but on the other hand provides no information on the dynamic balance between synthesis and degradation, which might differ considerably between HSPGs and CSPGs (32).

The Relative Expression Levels of extl3 and csgalnact1/csgalnact2 Influence the HS/CS Ratio—Both HS and CS are synthesized onto a common PG linkage tetrasaccharide. Interestingly, the saccharides in the linkage region may be modified by phosphorylation and sulfation to possibly affect whether predominantly HS or CS will be synthesized onto the linkage region (33–35). It has previously also been shown that domains present in PG core proteins influence the probability of modification by HS or CS (36). However, predicted purely from the biosynthetic scheme shown in Fig. 1, the activity or accessibility of enzymes adding either a GlcNAc (in the case of HS) or a GalNAc (in the case of CS) to the fourth sugar in the common linkage region will determine the type of GAG to be synthesized. Here, we show that the reduced initiation of HS biosynthesis in *extl3* mutants leads to increased CS accumulation (Fig. 3*A*) and that a reduction of CS initiation by targeting Csgalnact1 and Csgalnact2 function results in increased HS accumulation (Fig. 3*C*). We also find that siRNA-mediated suppression of Extl3 in HEK cells decreases the HS/CS ratio on a single GAG attachment site in Syndecan-4, compatible with a mechanism where Extl3 and GalnacT1/T2 compete for linkage regions or alternatively suggesting that linkage regions that are not used for HS biosynthesis may be used for CS biosynthesis (Fig. 4).

The present study also examined whether the mRNA expression levels of several core proteins and enzymes involved in HS and CS biosynthesis were perturbed in *extl3* mutant larvae. Whereas most of the investigated genes seems to be normally expressed in *extl3* larvae, the biglycan mRNA level was reduced as compared with wild type (Fig. 6). Although not significant, a trend for increased levels of aggrecan mRNA in *extl3* larvae was observed. This is interesting, because aggrecan may carry more than 100 CS chains per core protein unit. Because the lengths of CS chains in *extl3* mutants are indistinguishable from wild type (Fig. 5), it could be that the increased amounts of CS produced in these fish are present on core proteins that normally carry mostly HS (*e.g.*, syndecans) and/or that moderately elevated levels aggrecan also contribute to the increased CS levels. Based on the results presented here, we propose that the balance between *extl3* and *csgalnact1*/*csgalnact2* expression influences the HS/CS ratio, because these enzymes initiate HS and CS polymerization, respectively.

One additional explanation for the results obtained pertaining to the up-regulation of CS biosynthesis in *extl3* mutants and the up-regulation of HS biosynthesis in c*sgalnact1/csgalnact2* morphants could be that cells respond to the low HS or CS production *per se*. Interestingly, however, no increased CS accumulation was seen in *ext2* mutants despite a strong reduction in HS content (Fig. 3*A*), and no increased HS accumulation was seen in embryos injected with morpholinos targeting *chsy1* expression despite a strong reduction in CS content (Fig. 3*B*). This argues against the possibility of a feedback mechanism in response to reduced GAG levels.

Signaling in HS and CS Depleted Cartilages—The molecular mechanisms that cause chondrocytes in cartilages to flatten and arrange themselves into columns are probably conserved and ancient in vertebrates (supplemental Fig. S1). Several recent studies suggest that the intercalation of chondrocytes occurs by convergent extension where noncanonical frizzled signaling regulates cell polarity (37, 38). Wnt signaling has an important role in controlling the transition of resting chondrocytes to proliferative and hypertrophic chondrocytes (39). Defective *wnt5b* function results in a chondrocyte stacking phenotype, similar to what has been observed in *ext2* mutants (13). Recent studies also suggest that CS, in a fashion similar to HS, can influence Wnt signaling (40), and defects in chondro-

cyte stacking have been reported in mice with defective CS biosynthesis (41). It seems that defective Wnt signaling is likely to be part of the explanation for the observed defects in chondrocyte elongation and stacking in the GAG biosynthetic enzyme mutants investigated in the present study. However, it should be emphasized that the process of cartilage morphogenesis depends on a complex network of several types of paracrine signaling molecules, of which many if not all interact with HSPGs and in some cases also with CSPGs (42). In addition, there are many interactions between cells and the ECM where PGs play a central role (1, 2).

Different Effects on HS and CS Biosynthesis in uxs1 and b3gat3 Mutants—The reason(s) for why *uxs1* and *b3gat3* mutants still contain half of the normal HS content, whereas CS biosynthesis on the other hand is practically eliminated, needs to be discussed (Fig. 3*A*). Whereas the relative levels of the Extl3 and Csgalnact1/Csgalnact2 glycosyltransferases as shown here probably are important, there might still be other mechanisms that contribute to the molecular phenotypes in these mutants. One possibility is that chondrocytes in the *uxs1* and *b3gat3* mutants are unable to differentiate to a stage where normally large amounts of CS are efficiently produced and secreted, as indicated by the lack of maturation markers for chondrocytes in *uxs1* mutants (11). Another possibility could be that the maternal contribution of *uxs1* and *b3gat3* mRNA in the mutants is insufficient for the sudden scaling up of CS biosynthesis by certain subpopulations of cells (*e.g.*, chondrocytes) during chondrogenesis. Thus, the small residual amounts of CS detected at 6 dpf in *uxs1* and *b3gat3* mutants might have been mainly produced during the first days of zebrafish development. HS biosynthesis on the other hand occurs more evenly during embryo development (14), thereby potentially making more efficient use of the maternally contributed *uxs1* and *b3gat3* mRNA. Finally, it is also possible that alternative mechanisms yet to be identified exist to circumvent the lack of enzymatic activity in the respective mutants. For example, mechanisms for internalization and reglycanation of proteoglycans have been described (43) and would potentially provide a possibility for retaining some GAG biosynthesis in the mutants. If salvation pathways account for some of the GAGs detected in *uxs1* and *b3gat3* mutants or if other unknown mechanisms exist to compensate for the loss of GAG biosynthetic enzymatic activity in these mutants, such mechanisms might, however, be insufficient for the massive synthesis of CS to occur normally in chondrocytes.

Toward better Understanding of the Mechanisms behind MHE Onset—The results presented here could be of potential importance for understanding the biology behind the human disease multiple hereditary exostoses (MHE), also known as multiple osteochondromas. The mechanism for MHE onset is still debated (44). It is, however, generally accepted that mutations in either *EXT1* or *EXT2*, leading to decreased HS synthesis in the bone growth plates, result in chondrocytes that are able to escape proliferation control (45). Interestingly, in contrast to mutations in the human *EXT1* and *EXT2* genes, mutations in the human *EXTL3* gene have to our knowledge not been associated with MHE. Our study shows that zebrafish *extl3* mutants, in addition to increased CS production, produce more HS than *ext2* mutants. It is thus possible that the amounts of HS produced in *extl3* mutants are enough to retain proliferation control over chondrocytes, explaining why this gene has so far not been implicated with MHE onset. Another possibility raised by this study is that the observed overproliferation of chondrocytes found in MHE patients could not be due to decreased HS production *per se*, but instead is an effect of the abnormally sulfated HS produced by chondrocytes having two mutated *ext1* or *ext2* alleles. Our analysis of HS produced by *ext2* and *extl3* mutants showed a clear increase in the occurrence of highly sulfated ΔHexA2S-GlcNS6S HS disaccharides in these mutants (Fig. 7). This disaccharide species is often part of HS motifs that avidly interact with growth factors (46). Previous studies have suggested that EXT proteins are interacting with the HS sulfotransferases and thus affecting HS modification (47). Notably, zebrafish *uxs1* and *b3gat3* displayed the opposite tendency with a decrease in ΔHexA2S-GlcNS6S, indicating that the increased proportion of this disaccharide is not solely an effect of reduced HS biosynthesis but depends on which specific gene function has been altered (Fig. 7).

If the key to MHE onset relates to increased sulfation of HS, it is on the other hand difficult to understand why *extl3* mutations would not trigger the disease. Possibly, the increased CS production seen in this mutant could restore or normalize PG function, because CS has also been shown to have the capacity to impact growth factor signaling (40). At any rate, and in the light of our findings, it seems to be of great importance to analyze the GAG content of homozygous EXT1 and EXT2 mutant cells in tumor samples from patients with MHE to get a full view of the molecular phenotype. Finally, the data presented here underline the importance of GAG structural analysis to better understand the phenotypes arising from mutations in the different GAG biosynthetic enzymes, because at least to some extent there is an interplay between HS and CS biosynthesis.

Acknowledgments—We thank Professor Lena Kjellén for valuable discussions, Pancras C. W. Hogendoorn for sharing mutant lines, and Katrin Lundstedt-Enkel for statistical analysis.

REFERENCES

1. Kronenberg, H. M. (2003) Developmental regulation of the growth plate. *Nature* **423,** 332–336
2. Goldring, M. B., Tsuchimochi, K., and Ijiri, K. (2006) The control of chondrogenesis. *J. Cell Biochem.* **97,** 33–44
3. Kimmel, C. B., Miller, C. T., Kruze, G., Ullmann, B., BreMiller, R. A., Larison, K. D., and Snyder, H. C. (1998) The shaping of pharyngeal cartilages during early development of the zebrafish. *Dev. Biol.* **203,** 245–263
4. Yao, T., Ohtani, K., and Wada, H. (2008) Whole-mount observation of pharyngeal and trabecular cartilage development in lampreys. *Zoolog. Sci.* **25,** 976–981
5. Janvier, P., and Arsenault, M. (2007) The anatomy of *Euphanerops longaevus* Woodward, 1900, an anaspid-like jawless vertebrate from the Upper Devonian of Miguasha, Quebec, Canada. *Geodiversitas* **29,** 143–216
6. Kreuger, J., Spillmann, D., Li, J. P., and Lindahl, U. (2006) Interactions between heparan sulfate and proteins. The concept of specificity. *J. Cell Biol.* **174,** 323–327
7. Lin, X. (2004) Functions of heparan sulfate proteoglycans in cell signaling during development. *Development* **131,** 6009–6021
8. Kreuger, J., Perez, L., Giraldez, A. J., and Cohen, S. M. (2004) Opposing activities of Dally-like glypican at high and low levels of Wingless morphogen activity. *Dev. Cell* **7,** 503–512

9. LeClair, E. E., Mui, S. R., Huang, A., Topczewska, J. M., and Topczewski, J. (2009) Craniofacial skeletal defects of adult zebrafish Glypican 4 (knypek) mutants. *Dev. Dyn.* **238,** 2550–2563
10. Topczewski, J., Sepich, D. S., Myers, D. C., Walker, C., Amores, A., Lele, Z., Hammerschmidt, M., Postlethwait, J., and Solnica-Krezel, L. (2001) The zebrafish glypican knypek controls cell polarity during gastrulation movements of convergent extension. *Dev. Cell* **1,** 251–264
11. Eames, B. F., Singer, A., Smith, G. A., Wood, Z. A., Yan, Y. L., He, X., Polizzi, S. J., Catchen, J. M., Rodriguez-Mari, A., Linbo, T., Raible, D. W., and Postlethwait, J. H. (2010) UDP xylose synthase 1 is required for morphogenesis and histogenesis of the craniofacial skeleton. *Dev. Biol.* **341,** 400–415
12. Wiweger, M. I., Avramut, C. M., de Andrea, C. E., Prins, F. A., Koster, A. J., Ravelli, R. B., and Hogendoorn, P. C. (2011) Cartilage ultrastructure in proteoglycan-deficient zebrafish mutants brings to light new candidate genes for human skeletal disorders. *J. Pathol.* **223,** 531–542
13. Clement, A., Wiweger, M., von der Hardt, S., Rusch, M. A., Selleck, S. B., Chien, C. B., and Roehl, H. H. (2008) Regulation of zebrafish skeletogenesis by ext2/dackel and papst1/pinscher. *PLoS Genet.* **4,** e1000136
14. Lee, J. S., von der Hardt, S., Rusch, M. A., Stringer, S. E., Stickney, H. L., Talbot, W. S., Geisler, R., Nüsslein-Volhard, C., Selleck, S. B., Chien, C. B., and Roehl, H. (2004) Axon sorting in the optic tract requires HSPG synthesis by ext2 (dackel) and extl3 (boxer). *Neuron* **44,** 947–960
15. Schilling, T. F., Piotrowski, T., Grandel, H., Brand, M., Heisenberg, C. P., Jiang, Y. J., Beuchle, D., Hammerschmidt, M., Kane, D. A., Mullins, M. C., van Eeden, F. J., Kelsh, R. N., Furutani-Seiki, M., Granato, M., Haffter, P., Odenthal, J., Warga, R. M., Trowe, T., and Nüsslein-Volhard, C. (1996) Jaw and branchial arch mutants in zebrafish I. Branchial arches. *Development* **123,** 329–344
16. Walsh, E. C., and Stainier, D. Y. (2001) UDP-glucose dehydrogenase required for cardiac valve formation in zebrafish. *Science* **293,** 1670–1673
17. Neuhauss, S. C., Solnica-Krezel, L., Schier, A. F., Zwartkruis, F., Stemple, D. L., Malicki, J., Abdelilah, S., Stainier, D. Y., and Driever, W. (1996) Mutations affecting craniofacial development in zebrafish. *Development* **123,** 357–367
18. Grandel, H., Draper, B. W., and Schulte-Merker, S. (2000) Dackel acts in the ectoderm of the zebrafish pectoral fin bud to maintain AER signaling. *Development* **127,** 4169–4178
19. Norton, W. H., Ledin, J., Grandel, H., and Neumann, C. J. (2005) HSPG synthesis by zebrafish Ext2 and Extl3 is required for Fgf10 signalling during limb development. *Development* **132,** 4963–4973
20. Amsterdam, A., Nissen, R. M., Sun, Z., Swindell, E. C., Farrington, S., and Hopkins, N. (2004) Identification of 315 genes essential for early zebrafish development. *Proc. Natl. Acad. Sci. U.S.A.* **101,** 12792–12797
21. Lawson, N. D., and Weinstein, B. M. (2002) *In vivo* imaging of embryonic vascular development using transgenic zebrafish. *Dev. Biol.* **248,** 307–318
22. Westerfield, M. (1995) The zebrafish book. A guide for the laboratory use of zebrafish (*Danio rerio*). 4th Ed., Univ. of Oregon Press, Eugene, OR
23. van Eeden, F. J., Granato, M., Schach, U., Brand, M., Furutani-Seiki, M., Haffter, P., Hammerschmidt, M., Heisenberg, C. P., Jiang, Y. J., Kane, D. A., Kelsh, R. N., Mullins, M. C., Odenthal, J., Warga, R. M., and Nüsslein-Volhard, C. (1996) Genetic analysis of fin formation in the zebrafish, *Danio rerio*. *Development* **123,** 255–262
24. Ledin, J., Staatz, W., Li, J. P., Götte, M., Selleck, S., Kjellén, L., and Spillmann, D. (2004) Heparan sulfate structure in mice with genetically modified heparan sulfate production. *J. Biol. Chem.* **279,** 42732–42741
25. Zhang, J., Lefebvre, J. L., Zhao, S., and Granato, M. (2004) Zebrafish unplugged reveals a role for muscle-specific kinase homologs in axonal pathway choice. *Nat. Neurosci.* **7,** 1303–1309
26. Gopal, S., Bober, A., Whiteford, J. R., Multhaupt, H. A., Yoneda, A., and Couchman, J. R. (2010) Heparan sulfate chain valency controls syndecan-4 function in cell adhesion. *J. Biol. Chem.* **285,** 14247–14258
27. Prabhakar, V., and Sasisekharan, R. (2006) The biosynthesis and catabolism of galactosaminoglycans. *Adv. Pharmacol.* **53,** 69–115
28. Kitagawa, H., Uyama, T., and Sugahara, K. (2001) Molecular cloning and expression of a human chondroitin synthase. *J. Biol. Chem.* **276,** 38721–38726
29. Uyama, T., Kitagawa, H., Tanaka, J., Tamura, J., Ogawa, T., and Sugahara, K. (2003) Molecular cloning and expression of a second chondroitin *N*-acetylgalactosaminyltransferase involved in the initiation and elongation of chondroitin/dermatan sulfate. *J. Biol. Chem.* **278,** 3072–3078
30. Guo, S., Sato, T., Shirane, K., and Furukawa, K. (2001) Galactosylation of *N*-linked oligosaccharides by human β-1,4-galactosyltransferases I, II, III, IV, V, and VI expressed in Sf-9 cells. *Glycobiology* **11,** 813–820
31. Busse, M., Feta, A., Presto, J., Wilén, M., Grønning, M., Kjellén, L., and Kusche-Gullberg, M. (2007) Contribution of EXT1, EXT2, and EXTL3 to heparan sulfate chain elongation. *J. Biol. Chem.* **282,** 32802–32810
32. Esko, J. D., Kimata, K., and Lindahl, U. (2009) Proteoglycans and sulfated Glycosaminoglycans, in *Essentials of Glycobiology* (Varki, A., Cummings, R. D., Esko, J. D., Freeze, H. F., Stanely, P., Bertozzi, C. R., Hart, W. H., and Marilynn, E. E., eds) 2nd Ed., Cold Spring Harbor Laboratory, Cold Spring Harbor, NY
33. Tone, Y., Pedersen, L. C., Yamamoto, T., Izumikawa, T., Kitagawa, H., Nishihara, J., Tamura, J., Negishi, M., and Sugahara, K. (2008) 2-*O*-phosphorylation of xylose and 6-*O*-sulfation of galactose in the protein linkage region of glycosaminoglycans influence the glucuronyltransferase-I activity involved in the linkage region synthesis. *J. Biol. Chem.* **283,** 16801–16807
34. Gulberti, S., Lattard, V., Fondeur, M., Jacquinet, J. C., Mulliert, G., Netter, P., Magdalou, J., Ouzzine, M., and Fournel-Gigleux, S. (2005) Modifications of the glycosaminoglycan-linkage region of proteoglycans. Phosphorylation and sulfation determine the activity of the human β1,4-galactosyltransferase 7 and β1,3-glucuronosyltransferase I. *Sci. World J.* **5,** 510–514
35. Ueno, M., Yamada, S., Zako, M., Bernfield, M., and Sugahara, K. (2001) Structural characterization of heparan sulfate and chondroitin sulfate of syndecan-1 purified from normal murine mammary gland epithelial cells. Common phosphorylation of xylose and differential sulfation of galactose in the protein linkage region tetrasaccharide sequence. *J. Biol. Chem.* **276,** 29134–29140
36. Chen, R. L., and Lander, A. D. (2001) Mechanisms underlying preferential assembly of heparan sulfate on glypican-1. *J. Biol. Chem.* **276,** 7507–7517
37. Li, Y., and Dudley, A. T. (2009) Noncanonical frizzled signaling regulates cell polarity of growth plate chondrocytes. *Development* **136,** 1083–1092
38. Ahrens, M. J., Li, Y., Jiang, H., and Dudley, A. T. (2009) Convergent extension movements in growth plate chondrocytes require gpi-anchored cell surface proteins. *Development* **136,** 3463–3474
39. Yang, Y., Topol, L., Lee, H., and Wu, J. (2003) Wnt5a and Wnt5b exhibit distinct activities in coordinating chondrocyte proliferation and differentiation. *Development* **130,** 1003–1015
40. Nadanaka, S., Ishida, M., Ikegami, M., and Kitagawa, H. (2008) Chondroitin 4-*O*-sulfotransferase-1 modulates Wnt-3a signaling through control of E disaccharide expression of chondroitin sulfate. *J. Biol. Chem.* **283,** 27333–27343
41. Klüppel, M., Wight, T. N., Chan, C., Hinek, A., and Wrana, J. L. (2005) Maintenance of chondroitin sulfation balance by chondroitin-4-sulfotransferase 1 is required for chondrocyte development and growth factor signaling during cartilage morphogenesis. *Development* **132,** 3989–4003
42. Le Jan, S., Hayashi, M., Kasza, Z., Eriksson, I., Bishop, J. R., Weibrecht, I., Heldin, J., Holmborn, K., Jakobsson, L., Söderberg, O., Spillmann, D., Esko, J. D., Claesson-Welsh, L., Kjellén, L., and Kreuger, J. (2012) Functional overlap between chondroitin and heparan sulfate proteoglycans during VEGF-induced sprouting angiogenesis. *Arterioscler. Thromb. Vasc. Biol.* **32,** 1255–1263
43. Edgren, G., Havsmark, B., Jönsson, M., and Fransson, L. A. (1997) Glypican (heparan sulfate proteoglycan) is palmitoylated, deglycanated and reglycanated during recycling in skin fibroblasts. *Glycobiology* **7,** 103–112
44. Roehl, H. H., and Pacifici, M. (2000) Shop talk. Sugars, bones, and a disease called multiple hereditary exostoses. *Dev. Dyn.* **239,** 1901–1904
45. Jennes, I., Pedrini, E., Zuntini, M., Mordenti, M., Balkassmi, S., Asteggiano, C. G., Casey, B., Bakker, B., Sangiorgi, L., and Wuyts, W. (2009) Multiple osteochondromas. Mutation update and description of the multiple osteochondromas mutation database (MOdb). *Hum. Mutat.* **30,** 1620–1627
46. Kreuger, J., Jemth, P., Sanders-Lindberg, E., Eliahu, L., Ron, D., Basilico, C., Salmivirta, M., and Lindahl, U. (2005) Fibroblast growth factors share binding sites in heparan sulphate. *Biochem. J.* **389,** 145–150
47. Presto, J., Thuveson, M., Carlsson, P., Busse, M., Wilén, M., Eriksson, I., Kusche-Gullberg, M., and Kjellén, L. (2008) Heparan sulfate biosynthesis enzymes EXT1 and EXT2 affect NDST1 expression and heparan sulfate sulfation. *Proc. Natl. Acad. Sci. U.S.A.* **105,** 4751–4756